Highly wear-resistant and biocompatible carbon nanocomposite coatings for dental implants

Article *in* Biomaterials · June 2016

DOI: 10.1016/j.biomaterials.2016.06.029

7 authors, including:

Oleksiy V Penkov
Yonsei University
65 PUBLICATIONS **359** CITATIONS
SEE PROFILE

Vladimir Egorovich Pukha
National Technical University of Ukraine Kha…
29 PUBLICATIONS **74** CITATIONS
SEE PROFILE

Mahdi Khadem
Yonsei University
16 PUBLICATIONS **59** CITATIONS
SEE PROFILE

Vadym Starikov
Kharkiv Polytechnical Institute
55 PUBLICATIONS **144** CITATIONS
SEE PROFILE

Biomaterials 102 (2016) 130–136

Contents lists available at ScienceDirect

Biomaterials

journal homepage: www.elsevier.com/locate/biomaterials

Highly wear-resistant and biocompatible carbon nanocomposite coatings for dental implants

Oleksiy V. Penkov [a], Vladimir E. Pukha [b], Svetlana L. Starikova [c], Mahdi Khadem [a, d], Vadym V. Starikov [e], Maxim V. Maleev [e], Dae-Eun Kim [a, d, *]

[a] Center for Nano-Wear, Yonsei University, 120-749, Seoul, South Korea
[b] The Institute of Problems of Chemical Physics of the Russian Academy of Sciences, 142432, Chernogolovka, Russian Federation
[c] Kharkiv Medical Academy of Postgraduate Education, 61176, Kharkiv, Ukraine
[d] Department of Mechanical Engineering, Yonsei University, 120-749, Seoul, South Korea
[e] National Technical University, "Kharkiv Polytechnic Institute", 61002, Kharkiv, Ukraine

ARTICLE INFO

Article history:
Received 8 April 2016
Received in revised form
10 June 2016
Accepted 11 June 2016
Available online 15 June 2016

Keywords:
Carbon nanocomposite
Biocompatibility
Wear resistance
Dental implants
In vivo

ABSTRACT

Diamond-like carbon coatings are increasingly used as wear-protective coatings for dental implants, artificial joints, etc. Despite their advantages, they may have several weak points such as high internal stress, poor adhesive properties or high sensitivity to ambient conditions. These weak points could be overcome in the case of a new carbon nanocomposite coating (CNC) deposited by using a C_{60} ion beam on a Co/Cr alloy. The structure of the coatings was investigated by Raman and XPS spectroscopy. The wear resistance was assessed by using a reciprocating tribotester under the loads up to 0.4 N in both dry and wet sliding conditions. Biocompatibility of the dental implants was tested *in vivo* on rabbits. Biocompatibility, bioactivity and mechanical durability of the CNC deposited on a Co/Cr alloy were investigated and compared with those of bulk Co/Cr and Ti alloys. The wear resistance of the CNC was found to be 250–650 fold higher compared to the Co/Cr and Ti alloys. Also, the CNC demonstrated much better biological properties with respect to formation of new tissues and absence of negative morphological parameters such as necrosis and demineralization. Development of the CNC is expected to aid in significant improvement of lifetime and quality of implants for dental applications.

1. Introduction

The proper selection of an implant material is usually a complicated process because the biocompatibility must be assured together with sufficient durability and manufacturability of the material. Most commonly used metals exhibit low chemical passivity resulting in low biocompatibility and high corrosion of the surface [1–6]. Use of relatively passive ceramics is also limited because of their high brittleness [7]. These chemical and physical limitations lead to an increase in the thickness and geometrical dimensions of implants. It has been suggested that such issues may be overcome by development of appropriate composite materials [8–14]. However, the use of composite materials in implants introduces new challenges. A composite, while in contact with bone tissue, should exhibit high delamination stability, high adhesion and uniform contact [9–16]. Additionally, the coating and the substrate materials of an implant should have similar mechanical and physical properties such as thermal expansion coefficient and Young's modulus.

Development of carbon-based functional coatings for biomedical applications has been gaining increasing attention over the recent years. The use of carbon-based composites has significantly increased the wear resistance of implants [17–19]. Also, diamond-like carbon (DLC) coatings have recently received much attention because of their unique mechanical, chemical and thermal characteristics [20,21]. The combination of low friction and high wear resistant properties of DLC has increased the durability of precision components and friction pairs such as artificial joints [22]. Also, metallic implants with DLC coatings have demonstrated high biocompatibility [17,22]. Unlike other coating materials, DLC does not lead to blood coagulation. Instead, it effectively blocks the diffusion of metal ions, and therefore, it may be used to coat implants in contact with bone or soft tissues of the body. In fact,

* Corresponding author. Center for Nano-Wear, Yonsei University, 120-749, Seoul, South Korea.
E-mail address: kimde@yonsei.ac.kr (D.-E. Kim).

http://dx.doi.org/10.1016/j.biomaterials.2016.06.029
0142-9612/

carbon-based materials have demonstrated the ability to coalesce with surrounding tissues and to stimulate bone formation [23].

Non-hydrogenated DLC coatings can be deposited on different substrates by various methods, including sputtering [24], pulsed-laser deposition [25] or ion-beam deposition [26]. Each method has its own advantages as well as disadvantages such as high levels of internal stress, poor adhesive properties or high sensitivity to ambient conditions. These disadvantages of DLC coatings could be successfully overcome by using an accelerated fullerene ion beam during the deposition of carbon nanocomposite coatings (CNCs) [27–31]. The ion-beam deposition by using C_{60} fullerene molecules (instead of atomic carbon) allowed the formation of a new carbon-based material with unique nanocomposite structure and low level of internal stress [27,28], high adhesion to substrate [27] and low amount of defects [31]. The microstructure of CNC consisted of graphite nanocrystals embedded into an amorphous diamond-like matrix [29]. The graphite nanocrystals had a well-defined preferential orientation of graphene planes that were perpendicular to the surface [28]. It has been reported that the preferential orientation of the graphite nanocrystals plays an important role in the transition from biocompatibility of the coatings to their bioactivity, because of the sufficient difference in chemical and biochemical properties between the base and the edge directions of graphite crystals [32]. The nanocomposite structure also showed a relatively high ratio of hardness to Young's modulus, which led to better matching between the mechanical properties of the coating and a metallic substrate compared to DLC coatings deposited by traditional methods. Besides, thin DLC coatings usually have smooth surface and tend to reproduce the initial topography of the substrate [17]. CNCs deposited by the C_{60} ion beam showed unique nanoscale topography [29,30] that could be helpful for various biological applications [33,34].

For a number of reasons mentioned above, the CNC deposited by using a C_{60} ion beam could lead to the development of a new class of carbon coatings with excellent mechanical properties and biocompatibility. In this study, the most important requirements of a dental implant such as biocompatibility, bioactivity and wear resistance of the carbon nanocomposite coated on a Co/Cr alloy by C_{60} ion beam deposition technique were investigated and compared with those of bulk Co/Cr and Ti alloys. Methods used for specimen fabrication and experimental details are described in the following sections.

2. Materials and methods

2.1. Materials

Two types of metal alloys were used for preparation of the specimens: cobalt-chromium alloy, Vitallium (Co 62%, Cr 30%, Mo 5%, and C 0.4%) and titanium alloy, VT1-0 (Ti 99% and Fe 0.25%). Metallic plates with dimensions of $10 \times 15 \times 2$ mm^3 were used. C_{60}–fullerene powder (99.5% purity; NeoTechProducts, St. Petersburg, Russia) was used as the source material for the deposition of the CNCs.

2.2. Specimen preparation

CNCs were deposited on Co/Cr alloy plates by a C_{60} ion beam with an average ion energy of 7.5 keV. The deposition was performed in a modified vacuum setup (VUP-5M, Selmi, Ukraine) equipped with liquid-nitrogen traps. The base pressure was $1 \cdot 10^{-4}$ Pa, and the pressure of Ar during the deposition was $5 \cdot 10^{-3}$ Pa. Two oppositely directed ion beams were formed at the ion source with a saddle-shaped electric field. The first beam was used for monitoring and the second one was used for deposition. C_{60} vapor was supplied from two effusion cells, through a channel in the anode, directly to the saddle point of the electric field. The substrate temperature during the deposition was 250 °C.

Prior to loading the fullerene powders into the effusion cells, they were cleaned by vacuum distillation. Before the deposition, the loaded effusion cells were maintained under a high vacuum ($2 \cdot 10^{-4}$ Pa) at a temperature of 300 °C for 3 h. The temperature of the effusion cells during deposition was above 500 °C. For deposition of uniform coatings over a large area, the substrates were mounted on a holder that reciprocated back and forth across the ion beam. More detailed descriptions of the deposition process are available elsewhere [35,27].

2.3. Coating characterization

The structure and chemical composition of the coatings were investigated using scanning electron microscopy (SEM; Jeol 6210) in conjunction with energy-dispersive X-ray spectroscopy (OXFORD INCA Energy), Raman spectroscopy (LabRam Aramis) conducted at a wavelength of 532 nm, and X-ray photoelectron spectroscopy (XPS; Thermo Scientific K-Alpha). The thickness measurements were performed after deposition of the coating using a step method. Electrode potentials were measured using the standard AgCl electrode for rating the initial activity of metals [3]. The measurements were conducted in an electrochemical cell filled with physiological fluid (0.9% aqueous solution of NaCl). A standard AgCl reference electrode was used.

2.4. Friction and wear testing

A commercial reciprocating tribo-tester (CETR UMT-2) was used to investigate the wear behavior of the coating in both dry and wet sliding conditions. Artificial saliva (Xerostomia Saliva; Kalmar) was used as a media for the wet conditions. It should be noted that artificial saliva is commonly used for simulation of the actual biological environment in various dental experiments [36]. All experiments were performed under ambient temperature of approximately 25 °C and relative humidity of 45–55% in a Class 100 clean room. The sliding speed was set to 4 mm/s with a stroke of 2 mm, which corresponded to a sliding frequency of 1 Hz. Alumina balls with a diameter of 1 mm were chosen as the pins because of their high hardness and good chemical stability. An accelerated wear testing method was used to shorten the experiment time [37]. Thus, the loading conditions were selected to be much more severe compared to the actual biological environment. The normal load was set to either 50 mN or 400 mN, depending on the wear resistivity of the specimens. The corresponding maximum contact pressure was estimated using the Hertzian equation [38]. The repeatability of the experimental data was ensured by performing the sliding tests at least three times for each set of experimental conditions. A new pin was used for each experiment.

After the sliding tests, the amount of wear was assessed using a 3D laser microscope. The cross-sectional profiles of the wear tracks were mapped using a laser beam at a wavelength of 408 nm. The laser beam precisely scanned the specimen at a frame rate of 9 Hz with a high resolution of 1024×768 pixels. The normalized wear rate was then calculated by dividing the wear volume by the number of sliding cycles and the applied normal load.

2.5. Biocompatibility evaluation

Rabbits (20 months old with a body mass of approximately 3 kg) were separated into three groups for biocompatibility evaluation. Subperiosteal implants made of Co/Cr alloy, titanium alloy and nanocomposite-coated Co/Cr alloy were implanted in rabbits from

the first, second and third groups, respectively. Rabbits were sacrificed by air embolism at 12 weeks. The animal tests were performed according to the requirements of the European Convention and Ukrainian law.

After the rabbits were sacrificed, a fragment of the mandible, including the implant and a portion of the adjacent bone comprising an outer and an inner compact bone and spongy substance, was extracted. The extracted material was visually investigated using an optical microscope (Leica Axiostar Plus). For the microscopic investigation, the extracted fragments were fixed in 5 vol% nitric acid, then dehydrated in 96° ethanol and embedded into celloidin [39]. Cross-sections with thicknesses of 7–10 μm were colored with haematoxylin, eosin, and van Gieson's stain. Morphometric investigations were concentrated on the following characteristics: an estimation of the newly formed tissue between the parent compact bone and the implant; the presence of necrosis on the surface of the tissue adjacent to the implant; and assessment of the nature of the restructuring of the compact and trabecular bone [40].

2.6. Statistical analysis

For experiments in which there were at least three specimens investigated, statistical analysis was performed using the Student's t-test for two-tailed distributions with unequal variance. Significance in the statistical analysis was assigned for $p < 0.05$.

3. Results

3.1. Structure and mechanical properties of CNCs

Analysis of the 3D laser microscope data indicated that the thickness of the coating was approximately 300 nm. The surface roughness (RMS) of the coatings was obtained by averaging the roughness values of 5 random areas (100 μm × 100 μm) on the specimen surface. The average roughness value was determined to be approximately 50 nm.

The properties of carbon coatings are known to be significantly affected by their nanostructure. In particular, the hardness of the carbon coating is largely determined by the concentration of sp^3 bonds. Ratio of sp^2 and sp^3 bonds in the surface layers was determined directly by XPS analysis (Fig. 1a). Multi-peak fitting with the Gauss-Lorentz function was used to determine the C_{1s} peak components. The C_{1s} peak consisted of one major peak located at 284.9 eV that corresponded to sp^3 bonds and a minor peak at 284 eV which represented sp^2 bonds [41]. The smaller side peaks represented the C–O and C(O)O compounds [42]. It should be noted that oxygen was not incorporated during the deposition process. Estimation of the absorption/desorption ratio [43] showed that the amount oxygen atoms incorporated into the film during deposition was quite negligible. Moreover, impact of energetic C_{60} ions led to the formation of acoustic waves resulting in desorption of oxygen from the surface [44]. Therefore, the presence of these low-intensity oxygen compound peaks could be attributed to the surface absorption of oxygen in the atmosphere [45]. The percentage of sp^3 content was then calculated by taking the area beneath the sp^3 peaks and dividing it by the total area beneath the sp^2, sp^3 peaks. The results indicated that the sp^3 concentration was ~67%.

Besides XPS, Raman analysis (Fig. 1b) was used for detailed investigation of the nanostructure of DLC coatings. The Raman spectrum for the CNC is shown in Fig. 1b. The spectrum was typical of amorphous carbon and contained two peaks (referred to as D and G components) between 1,000 and 1,800 cm^{-1}. The exact positions of these components were calculated by fitting the

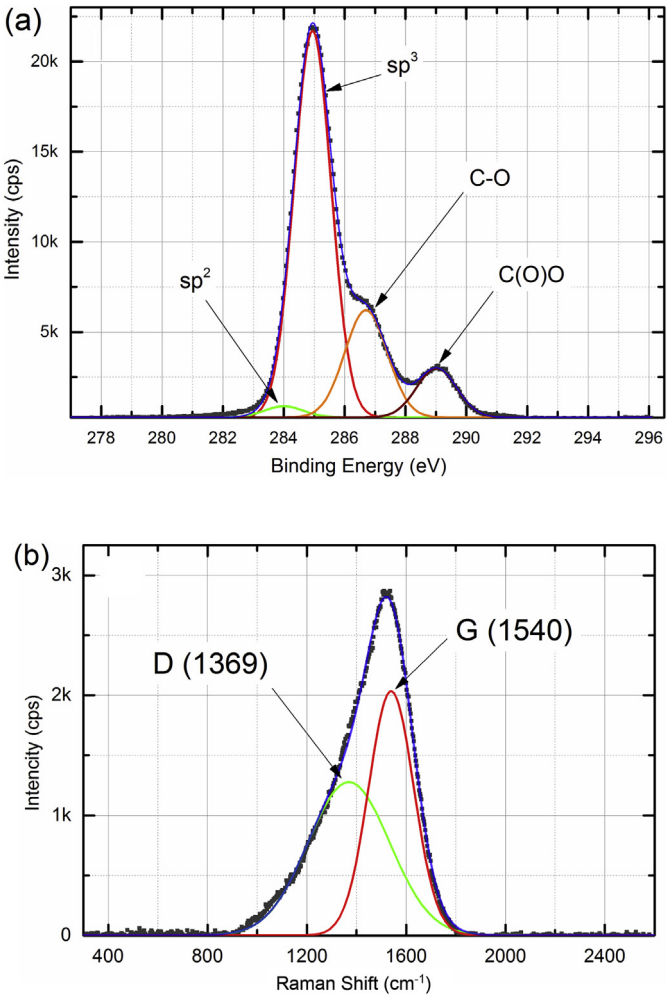

Fig. 1. a) XPS spectra of the CNC-Co/Cr specimen. sp^2 peak at 284 eV, sp^3 peak at 284.9 eV, C–O peak at 286.6 eV and C(O)O at 289 eV b) Raman spectra of the CNC-Co/Cr specimen. D-peak at 1369 cm^{-1} and G-peak at 1540 cm^{-1}.

spectrum to a Gaussian function. The fitting results indicated that the G peak was positioned at 1,540 cm^{-1}. The I(D)/I(G) ratio was approximately 0.6. To interpret this result correctly, it should be taken into account that under the excitation by visible light only the configuration of sp^2 bonds could be characterized, and the concentration of sp^3 bonds could not be determined directly. The presence of D and G components in the spectrum corresponded to a "breathing" mode (i.e., a benzene-ring vibration in which the diameter of the hexagonal structure changes) and a "stretching" mode (i.e., vibrations of sp^2 carbon chains and benzene rings stretching in one direction and compressing in the other), respectively. These processes were related to the state of sp^2 bonds.

The position of the G-peak is affected by several structural factors such as the degree of disorder, presence of sp^2 chains and clustering. The same factors are related to the concentration of sp^3 bonds for DLC films deposited by accelerated carbon atoms under room temperature. In this case, based on the model first proposed by Ferrari and Robertson [46], the concentration of sp^3 bonds in the coatings could be estimated based on the ratio of the intensities of the D and G peaks and the shift in the position of the G peak. In the case of the CNCs deposited by the C_{60} ion beam, the relation between the sp^3 content and parameters of the D and G peaks was more complicated. The calculation based on the Ferrari and Robertson model showed approximately 15% lower concentration of

the sp^3 bonds compared to the XPS data and the estimation based on the mechanical properties of the coatings. The concentration of the sp^3 bonds was also estimated using an empirical formula proposed by Cui et al. [47]. This estimation was based on the full-width at half-maximum (FWHM) of the G peak. The FWHM(G) was approximately 214 cm^{-1}, corresponding to a 65% concentration of sp^3 bonds, which was in good agreement with the estimation provided by the XPS data.

Mechanical properties of the coating were assessed by using the ultra-nano hardness testing method. The typical indentation curve is shown in Supplementary Fig. S1. To avoid the substrate effect, the indentation depth was maintained to be below 10% of the coating thickness. Assuming the coating thickness of 300 nm, the maximum indentation depth was set to 30 nm. The values of hardness and Young's modulus were calculated to be 45 GPa and 417 GPa, respectively. Thus, the mechanical properties of the films also indicated a high concentration of sp^3 bonds. Comparison between the XPS data and the estimation based on the mechanical properties showed that FWHM (G) was the important characteristic of the CNC which allowed the assessment of the amount of sp^3 bonds.

The electrode potentials of all the specimens are shown in Fig. S2. The lowest potential was exhibited by the bare Co/Cr alloy. At the start of the test, the potential dropped to −0.32 V and then gradually increased to −0.15 V. Bare titanium exhibited a higher potential of approximately 0.05 V. The CNC deposited on the Co/Cr alloy exhibited a positive potential during the tests; it slightly decreased to 0.07 V during the first 3 min and then increased to 0.2 V.

3.2. Wear resistance

Sliding tests were performed using a reciprocating tribo-tester to assess the friction and wear properties of the specimens. The sliding tests were performed for 3,600 cycles under a normal load of 50 mN for the bare Ti and Co/Cr alloys and 400 mN for the CNC-Co/Cr specimen. A higher load was used for the coated specimen based on its higher wear resistance as observed in a previous work [27]. The contact stresses calculated by the Hertzian equation for the normal loads of 50 mN and 400 mN were approximately 950 MPa and 1.8 GPa, respectively. The variation in the coefficient of friction (COF) of the specimens with respect to sliding cycles after three repeated tests, in dry and wet sliding conditions are shown in Fig. 2a and b, respectively. In dry conditions (Fig. 2a), the average COFs for the bare Ti and Co/Cr alloy specimens were 0.82 and 0.47, respectively. However, the CNC-Co/Cr specimen showed a much lower COF of 0.1 compared to the bare alloy specimens. In wet conditions (Fig. 2b), the bare Ti and CoCr alloy specimens showed relatively lower COFs of 0.43 and 0.38, respectively. The CNC-CoCr specimen showed a slightly lower COF of 0.09 compared to the dry sliding condition. The COF of the CNC-CoCr specimen was almost the same under 50 and 400 mN loads in both dry and wet sliding conditions. Fig. 3a and b summarize and compare the mean COF values together with their deviations for all the specimens in dry and wet sliding conditions for both normal loads.

In order to assess the lifetime of the CNC-Co/Cr specimen extended sliding tests (72,000 cycles; 20 h) were performed. The extended sliding tests were performed in dry sliding condition rather than the wet condition in order to accelerate the wear process. The coated specimen exhibited a very stable COF with no significant fluctuation, indicating the presence of the CNC at the contact interface, even after a large number of cycles under a normal load of 400 mN (Fig. S3). The COF maintained a low value of 0.1 up to approximately 60,000 cycles, which corresponded to approximately 17 h of sliding. Beyond 60,000 cycles, the COF started to increase and reached a value of about 0.24 after 73,000 cycles, which indicated the gradual removal of the CNC from the contact interface.

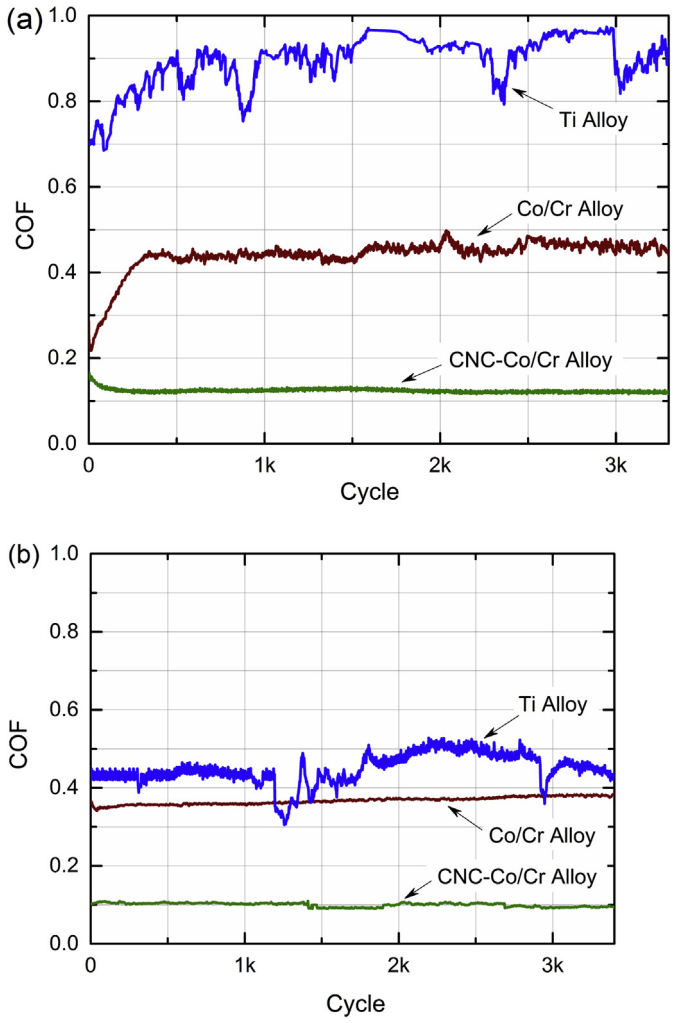

Fig. 2. Coefficient of friction with respect to sliding cycles for the bare Ti and Co/Cr alloy specimens under the normal load of 50 mN and the CNC-Co/Cr specimen under the normal load of 400 mN in (a) dry and (b) wet conditions.

The wear resistance of the specimens was evaluated after the sliding tests. The amount of wear was expressed as a normalized wear rate that was obtained by dividing the wear volume by the number of sliding cycles and the applied normal load [48]. The mean wear rate values together with their deviations for all the specimens in dry and wet sliding conditions are shown in Fig. 4. In dry conditions, the wear rates for the Ti and Co/Cr alloy were 1.3×10^{-7} $mm^3/N \cdot mm$ and 8.8×10^{-8} $mm^3/N \cdot mm$, respectively. The CNC-Co/Cr specimen showed a significantly lower wear rate of 3.2×10^{-10} $mm^3/N \cdot mm$. The deposition of CNC on the Co/Cr alloy resulted in approximately 100-fold decrease in the wear rate compared to that of the bare Co/Cr specimen. Moreover, the coated specimen exhibited a wear rate of approximately 400 times lower than that of the Ti alloy specimen. As expected, the specimens showed relatively lower wear rates in wet sliding conditions. The corresponding wear rates for the Ti alloy, Co/Cr alloy and CNC-Co/Cr were 7×10^{-8} $mm^3/N \cdot mm$, 3.8×10^{-8} $mm^3/N \cdot mm$, and 1.1×10^{-10} $mm^3/N \cdot mm$, respectively.

In order to better understand the wear behavior of the CNC-Co/Cr specimen, the amount of wear was evaluated at different

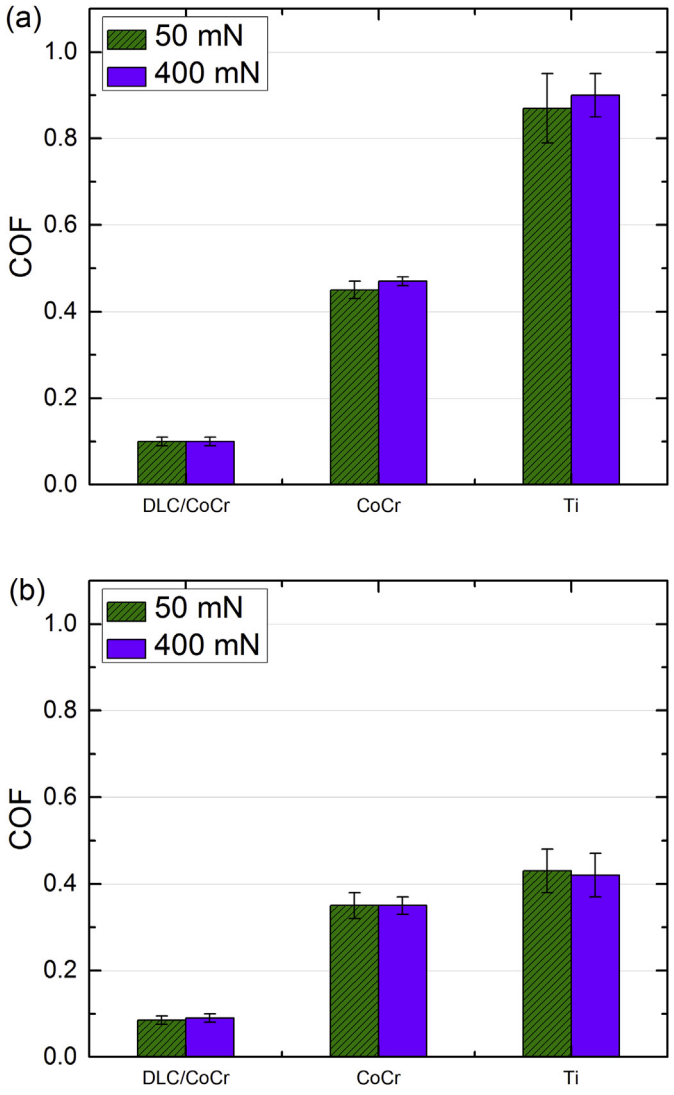

Fig. 3. Comparison of the average COF values of bare Co/Cr and Ti alloy specimens and CNC-Co/Cr specimen for different normal loads in (a) dry and (b) wet conditions.

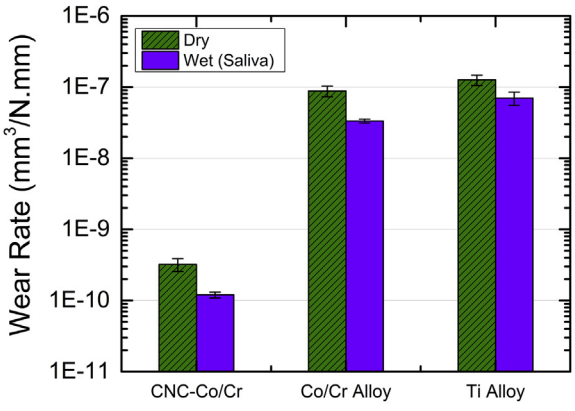

Fig. 4. Comparison of the wear rates of bare Co/Cr and Ti alloy specimens and CNC-Co/Cr specimen.

number of sliding cycles. Fig. S4 shows the 3D laser microscope and SEM images together with the 2D cross-sectional profiles of the wear tracks of the CNC-Co/Cr specimen after 36,000 (Fig. S4a) and 72,000 (Fig. S4b) sliding cycles. The width and depth of the wear track increased from ~75 μm to ~250 nm, respectively, to ~90 μm and ~1 μm as the number sliding cycles increased from 36,000 to 72,000. From this result, it was determined that the depth of wear became greater than the thickness of the nanocomposite coating after 72,000 cycles, which indicated that the coating was completely removed between 36,000 and 72,000 cycles. Considering the sudden increase in the COF data after 60,000 cycles, it could be postulated that failure of the coating occurred at this point.

3.3. Biocompatibility

3.3.1. Co/Cr alloy

Biocompatibility of the specimens was analyzed by optical microscopy of the specimens extracted from the rabbits after 12 weeks of implantation. Microscopic investigation revealed that the Co/Cr alloy implant was firmly adhered to the surface of the bone and was partially covered by connective tissues. Connective tissue sections with a high density of fibroblasts were observed in the areas between the implant and compact jaw bone (Fig. S5a, b). At other locations, the implant was in direct contact with the parent bone. In these areas, the bone tissue exhibited signs of destructive disorders such as absence of osteocytes, presence of demineralization niduses, and chaotic arrangement of basophilic resting lines. Also, small foci of cellular detritus were observed, as were compact bone restructuring areas with small resorption cavities. These cavities were filled with loose connective tissues. Narrow basophilic resting lines of bone remodeling foci and strata between the bone tissues were also observed. The morphological parameters of the mandible after implantation of the Co/Cr alloy plates are shown in Table 1.

3.3.2. Ti alloy

The microscopic investigation of compact bone sites adjacent to the Ti alloy implant revealed areas of newly formed, mature bone. This bone was observed with connective tissues, a low density of fibroblasts and bundles of collagen fibers (Fig. S6a, b). Isolated foci of necrosis between the implant and the newly formed tissue were observed. Evidence of restructuring processes was observed in the compact bone of the jaw near the surface of the implant. These processes required the formation of resorption cavities, which were filled with friable connective tissue with a high density of capillary-type blood vessels. The density of osteoblasts was increased in the edge regions of trabecula of the cancellous bone. Intertrabecular spaces were also filled with friable connective tissues.

3.3.3. CNC-Co/Cr alloy

The microscopic investigation showed that edge surfaces of the implant were covered with connective tissues. Fields with rough bone were primarily observed between the implant and the compact body of the jaw bone. Only small areas containing connective tissues with collagen fibers arranged parallel to the surface of the implant were evident. Only single, mature fibroblasts were observed (Fig. 5).

Resorption cavities were observed in compact bone areas located under the implant. These cavities exhibited various shapes and sizes and were filled with friable connective tissues or bone marrow fat. Some signs of restructuring, which included the formation of basophilic resting lines, were observed. These resting lines separated the strata and the newly formed bone. These areas contained a high density of osteoblasts (Table 1).

Table 1
Gradation of severity of morphological parameters of the mandible body for rabbits in 12 weeks after implantation.

Indicator	Gradation	Implant type		
		Co/Cr alloy	Titanium alloy	DLC on Co/Cr
		Severity		
Newly formed tissue between parent compact bone and implant	Connective tissue, %	89.67 ± 0.88	76.33 ± 4.30	69.33 ± 4.80
	Coarse-fibered bone, %	10.33 ± 0.88	23.67 ± 4.40	31.66 ± 1.76
Foci of necrosis at the tissue surface adjacent to the implant	Absence	–	–	+
	Isolated foci	+	+	–
	1/3 of the contact surface	–	–	–
The nature of the compact bone restructuring	Osteocyte-free area	0.33	0.33	0.25
	Resorption cavity, %	50.70 ± 2.60	44.67 ± 2.60	41.67 ± 3.33
	Demineralization foci	Single	Single	Absent
Characteristics of trabecular bone reconstruction	Density of Osteocytes	119.33 ± 1.20	122.00 ± 6.43	158.00 ± 1.15
	Expanded intertrabecular space, %	61.00 ± 4.36	57.30 ± 4.40	43.67 ± 2.60

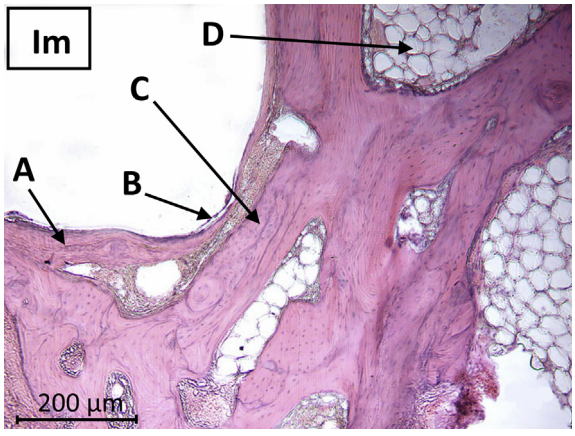

Fig. 5. Microscopy of carbon nanocomposite-coated implant (Im), fragment of the jaw bone: A – Coarse-fibered bone tissue around the perimeter of the implant; B – Narrow strips of connective tissue; C – Basophilic glue line; D – Generation of newly formed bone. The specimen was painted with haematoxylin and eosin.

4. Discussion

The experimental results showed that CNC deposited on Co/Cr alloy by using the C_{60} ion beam deposition process could significantly enhance the biocompatibility and durability of the implant. In the case of durability, the coated specimen showed up to 100-fold higher wear resistance than the bare Co/Cr alloy. This remarkable result was achieved despite the fact that the C_{60} ion beam deposition process used in this work was significantly simplified compared to the process reported previously [27,35]. The deposition was performed without the use of a mass separator to reduce the cost and time of the process. The durability of the CNC-Co/Cr alloy was sufficiently high to be applied in biomedical implant applications. Furthermore, the use of the ion beam permitted the coating of structures with complex shapes.

The lifetime of the CNC-Co/Cr alloy implant in actual biological environment may be predicted by using the Archard's wear model [38]. The number of cycles to failure, N_F, could be estimated by the following equation based on the Archard's law:

$$N_F = \frac{A \cdot H}{2 \cdot k \cdot F} \quad (1)$$

where A is the wear area, H is the hardness, k is the wear coefficient and F is the applied normal load. The experimental wear coefficient for the CNC-CoCr alloy was approximately 1×10^{-8}. The wear area could be estimated geometrically by assuming the diameter of the pin and the maximum wear depth, which was considered to be equal to the thickness of the coating. The normal load experienced in an actual biological environment could be estimated by the Hertzian contact theory [38] based on the maximum contact stress. According to previous reports, the maximum contact stress experienced by dental implants in human is in the range of 50–160 MPa [49,50]. Taking into account the material and diameter of the pin, it was found that this contact stress corresponded to a normal load, F, of about 0.1 mN. By substituting these values into eq. (1), it could be found that the predicted number of cycles to failure exceeded 1 billion. Thus, it may be stated that the CNC coated CoCr implant has sufficient mechanical durability for real application.

As for the corrosion resistance, the coated specimen exhibited a higher electrode potential compared with those of the bare metal alloy specimens. The high positive electrode potential indicated that the material exhibited good resistance to electrochemical degradation. This observation was in good agreement with the previous work by Lee et al. [51] regarding the chemical stability of carbon coatings deposited by a C_{60} ion beam. It was shown that these coatings exhibit excellent corrosion resistance in aggressive anodic and cathodic environments.

In regard to biocompatibility, the coated specimen proved to be superior compared to the metal alloy specimens. In all cases, complex reparative and adaptive-compensatory mutations occurred after implantation in compact and spongy bone. The severity of these mutations depended on the type of implant material. However, CNC deposited by the C_{60} ion beam on the Co/Cr alloy significantly improved the durability of implants and increased their acclimation rate. Furthermore, the benefits of the CNC with respect to formation of new tissues were demonstrated. The density of coarse-fibered bone tissue between the implant and the compact bone, as well as the number of osteocytes and the reduced density of resorption lacunae were maximized. In contrast, average characteristics were shown by the Ti implant and negative results were found for the uncoated Co/Cr alloy implant.

5. Conclusions

The structural, mechanical and biological properties of carbon nanocomposite coatings deposited by the C_{60} ion beam on a Co/Cr alloy were assessed. The properties of coated alloys were compared with those of bare Ti and Co/Cr alloy. It was found that the nanocomposite coated Co/Cr alloy exhibited high wear resistance accompanied by high biocompatibility when tested on rabbits. The wear resistance of the coated alloy was 100–400 fold higher compare to bare Co/Cr and Ti alloys. Besides superior durability, the nanocomposite coating demonstrated better biological properties with respect to formation of new tissues and absence of negative

morphological parameters such as necrosis and demineralization. On the basis of these results, it may be stated that deposition of carbon nanocomposite coating on Co/Cr alloy by a C_{60} ion beam is a promising technology for orthopedic and dental applications.

Acknowledgments

This work was supported by a National Research Foundation of Korea (NRF) grant funded by the Korea government (MSIP) (No. 2010-0018289).

Appendix A. Supplementary data

Supplementary data related to this article can be found at http://dx.doi.org/10.1016/j.biomaterials.2016.06.029.

References

[1] S.L. Rice, S.F. Wayne, W.F. Bailey, M. Roto, Influence of variation in contact stress on the sliding-wear behaviour of a dental amalgam, Biomaterials 2 (1981) 46–48.
[2] J. Rieu, A. Pichat, L.M. Rabbe, A. Rambert, C. Chabrol, M. Robelet, Ion implantation effects on friction and wear of joint prosthesis materials, Biomaterials 12 (1991) 139–143.
[3] V.V. Starikov, S.L. Starikova, A.G. Mamalis, S.N. Lavrynenko, J.J. Ramsden, The application of niobium and tantalum oxides for implant surface passivation, J. Bio Phys. Chem. 7 (2007) 141–145.
[4] D. Iijima, T. Yoneyama, H. Doi, H. Hamanaka, N. Kurosaki, Wear properties of Ti and Ti–6Al–7Nb castings for dental prostheses, Biomaterials 24 (2003) 1519–1524.
[5] J.J. Lee, I.S. Park, G.S. Shin, S.K. Lyu, S.G. Ahn, T.S. Bae, et al., Effects of polydopamine coating on the bioactivity of titanium for dental implants, Int. J. Precis. Eng. Man. 15 (2014) 1647–1655.
[6] I.S. Park, T.S. Bae, The bioactivity of enhanced Ti-32Nb-5Zr alloy with anodic oxidation and cyclic calcification, Int. J. Precis. Eng. Man. 15 (2014) 1595–1600.
[7] L. Guehennec, P. Layrolle, G. Daculsi, A review of bioceramics and fibrin sealant, Eur. Cells Mater. 8 (2004) 1–11.
[8] M. Atai, E. Yassini, M. Amini, D.C. Watts, The effect of a leucite-containing ceramic filler on the abrasive wear of dental composites, Dent. Mater. 23 (2007) 1181–1187.
[9] S. Ramakrishna, J. Mayer, E. Wintermantel, K.W. Leong, Biomedical applications of polymer-composite materials: a review, Compos. Sci. Technol. 61 (2001) 1189–1224.
[10] W.M. Bok, S.Y. Kim, S.J. Lee, G.S. Shin, J.M. Park, M.H. Lee, Surface characteristics and bioactivation of sandblasted and acid-etched (SLA) Ti-10Nb-10Ta alloy for dental implant, Int. J. Precis. Eng. Man. 16 (2015) 2185–2192.
[11] Z.B. Luklinska, W. Bonfield, Morphology and ultrastructure of the interface between hydroxyapatite-polyhydroxybutyrate composite implant and bone, J. Mater. Sci. Mater. Med. 8 (1997) 379–383.
[12] T. Elangovan, R.P. George, P. Kuppusami, D. Mangalaraj, S. Bera, E. Mohandas, et al., Development of a CrN/Cu nanocomposite coating on titanium-modified stainless steel for antibacterial activity against Pseudomonas aeruginosa, Biofouling 28 (2012) 779–787.
[13] Y.F. Huang, J.Z. Xu, J.S. Li, B.X. He, L. Xu, Z.M. Li, Mechanical properties and biocompatibility of melt processed, self-reinforced ultrahigh molecular weight polyethylene, Biomaterials 35 (2014) 6687–6697.
[14] W.M. Palin, G.J. Fleming, F.J. Burke, P.M. Marquis, M.R. Pintado, R.C. Randall, et al., The frictional coefficients and associated wear resistance of novel low-shrink resin-based composites, Dent. Mater. 21 (2005) 1111–1118.
[15] N.C. Lawson, D. Cakir, P. Beck, M.S. Litaker, J.O. Burgess, Characterization of third-body media particles and their effect on in vitro composite wear, Dent. Mater. 28 (2012) e118–e126.
[16] C.F. Huang, H.C. Cheng, Y. Lin, C.W. Wu, Y.K. Shen, Study on cellar behaviors on different nanostructures by nanoporous alumina template, Int. J. Precis. Eng. Man. 15 (2014) 689–693.
[17] A. Grill, Diamond-like carbon coatings as biocompatible materials—an overview, Diam. Relat. Mater. 12 (2003) 166–170.
[18] R. Hauert, A review of modified DLC coatings for biological applications, Diam. Relat. Mater. 12 (2003) 583–589.
[19] J.R. Queiroz, P.H. Corazza, A.M. Silva, S.M. Marocho, R.O. Souza, M.A. Bottino, Carbon film coating abutment surface: effect on the screw detorque, Dent. Mater. 28 (Supplement 1) (2012) e33–e34.
[20] A. Erdemir, C. Donnet, Tribology of diamond-like carbon films: recent progress and future prospects, J. Phys. D 39 (2006) R311–R327.
[21] J.R. Queiroz, S.F. Fissmer, C.Y. Ito, A.C. Salvia, M. Massi, L. Nogueira Junior, Effect of DLC film on C. albicans biofilm formation, Dent. Mater 26 (Supplement 1) (2010) e80.
[22] G. Dearnaley, J.H. Arps, Biomedical applications of diamond-like carbon (DLC) coatings: a review, Surf. Coat. Technol. 200 (2005) 2518–2524.
[23] M. Allen, B. Myer, N. Rushton, In vitro and in vivo investigations into the biocompatibility of diamond-like carbon (DLC) coatings for orthopedic applications, J. Biomed. Mater. Res. 58 (2001) 319–328.
[24] J. Deng, M. Braun, Residual stress and microhardness of DLC multilayer coatings, Diam. Relat. Mater. 5 (1996) 478–482.
[25] M. Jelinek, K. Smetana, T. Kocourek, B. Dvorankova, J. Zemek, J. Remsa, et al., Biocompatibility and sp3/sp2 ratio of laser created DLC films, Mater. Sci. Eng. B 169 (2010) 89–93.
[26] M.M. Morshed, B.P. McNamara, D.C. Cameron, M.S. Hashmi, Stress and adhesion in DLC coatings on 316L stainless steel deposited by a neutral beam source, J. Mater. Process. Tech. 143–144 (2003) 922–926.
[27] O.V. Penkov, V.E. Pukha, E.N. Zubarev, S.S. Yoo, D.E. Kim, Tribological properties of nanostructured DLC coatings deposited by C60 ion beam, Tribol. Int. 60 (2013) 127–135.
[28] V.E. Pukha, E.N. Zubarev, A.N. Drozdov, A.T. Pugachov, S.H. Jeong, S.C. Nam, Growth of nanocomposite films from accelerated C 60 ions, J. Phys. D 45 (2012) 335302–335309.
[29] V.E. Pukha, V.L. Karbovskii, A.N. Drozdov, A.T. Pugachov, Electronic properties and structure of carbon nanocomposite films deposited from accelerated C 60ion beam, J. Phys. D 46 (2013) 485305–485308.
[30] M. Khadem, O.V. Penkov, V.E. Pukha, M.V. Maleyev, D.E. Kim, Ultra-thin nanopatterned wear-protective diamond-like carbon coatings deposited on glass using a C60 ion beam, Carbon 80 (2014) 534–543.
[31] V.E. Pukha, V.L. Karbovskii, S.O. Rudchenko, A.N. Drozdov, M.V. Maleyev, V.V. Starikov, et al., Electronic and optical properties of superhard nanocomposite films obtained from C 60 ion beam, Mater Res. Express 1 (2014) 035049–035111.
[32] G. Zhang, P.M. Kirkman, A.N. Patel, A.S. Cuharuc, K. McKelvey, P.R. Unwin, Molecular functionalization of graphite surfaces: basal plane versus step edge electrochemical activity, J. Am. Chem. Soc. 136 (2014) 11444–11451.
[33] A.V. Singh, R. Patil, D.K. Thombre, W.N. Gade, Micro-nanopatterning as tool to study the role of physicochemical properties on cell–surface interactions, J. Biomed. Mater. Res. A 101 (2013) 3019–3032.
[34] T.C. Lowe, R.A. Reiss, Understanding the biological responses of nanostructured metals and surfaces, IOP Conf. Ser. 63 (2014) 012172–012175.
[35] V.E. Pukha, A.T. Pugachov, N.P. Churakova, E.N. Zubarev, V.E. Vinogradov, S.C. Nam, Synthesis, structure and properties of superhard nanostructured films deposited by the C60 ion beam, J. Nanosci. Nanotechnol. 12 (2012) 4762–4768.
[36] J.C. Souza, M. Henriques, W. Teughels, P. Ponthiaux, J.P. Celis, L.A. Rocha, Wear and corrosion interactions on titanium in oral environment: literature review, J. Bio Tribo Corros. 1 (2015) 1–13.
[37] S.H. Lee, S.S. Yoo, D.E. Kim, B.S. Kang, H.E. Kim, Accelerated wear test of FKM elastomer for life prediction of seals, Polym. Test. 31 (2012) 993–1000.
[38] K.L. Johnson, Contact Mechanics, Cambridge University Press, Cambridge, 1985.
[39] R.G. Kessel, Basic Medical Histology: The Biology of Cells, Tissues, and Organs, Oxford University Press, New York, 1998.
[40] J.A. Oort, J.P. Baak, A Manual of Morphometry in Diagnostic Pathology, Springer-Verlag, Berlin, 2011.
[41] J. Diaz, G. Paolicelli, S. Ferrer, F. Comin, Separation of the sp3 and sp2 components in the C1s photoemission spectra of amorphous carbon films, Phys. Rev. B 54 (1996) 8064–8069.
[42] S. Yumitori, Correlation of C1s chemical state intensities with the O1s intensity in the XPS analysis of anodically oxidized glass-like carbon samples, J. Mater. Sci. 35 (2016) 139–146.
[43] L. Maissel, R. Glang, Handbook of Thin Film Technology, McGraw-Hill, New York, 1970.
[44] R. Webb, Energetic cluster induced desorption from a graphite surface, Appl. Surf. Sci. 231 (2004) 59–63.
[45] S. Nakao, K. Yukimura, S. Nakano, H. Ogiso, DLC coating by HiPIMS: the influence of substrate bias voltage, Plasma Sci. 41 (2013) 1819–1829. IEEE Transactions on.
[46] A.C. Ferrari, A. Libassi, B.K. Tanner, V. Stolojan, J. Yuan, L.M. Brown, et al., Density, sp^3 fraction, and cross-sectional structure of amorphous carbon films determined by X-ray reflectivity and electron energy-loss spectroscopy, Phys. Rev. B 62 (2000) 11089–11103.
[47] W.G. Cui, Q.B. Lai, L. Zhang, F.M. Wang, Quantitative measurements of sp3 content in DLC films with Raman spectroscopy, Surf. Coat. Technol. 205 (2010) 1995–1999.
[48] O.V. Penkov, A.Y. Devizenko, M. Khadem, E.N. Zubarev, V.V. Kondratenko, D.E. Kim, Toward zero micro/macro-scale wear using periodic nano-layered coatings, ACS App. Mater. Interface 7 (2015) 18136–18144.
[49] S. Rajendran, M. Shamnadh, P. Dileep, Stress analysis of dental implants, J. Dent. Implants 4 (2016) 115–116.
[50] S.E. Quaresma, P.R. Cury, W.R. Sendyk, C. Sendyk, A finite element analysis of two different dental implants: stress distribution in the prosthesis, abutment, implant, and supporting bone, J. Oral Implant. 34 (2008) 1–6.
[51] S.H. Lee, V.E. Pukha, V.E. Vinogradov, N. Kakati, S.H. Jee, S.B. Cho, et al., Nanocomposite-carbon coated at low-temperature: a new coating material for metallic bipolar plates of polymer electrolyte membrane fuel cells, Int. J. Hydrogen Energ. 38 (2013) 14284–14294.